



Synthesis, characterization, and application of ZIF-8 for removal of Cd, Ni, and Pb ions from aqueous solutions: Optimization of the process by Response Surface Methodology (RSM) based on Central Composite Design (CCD) technique

Amir KHOSRAVI¹, Maryam RANDJBAR^{1,*}, and Razieh HABIBPOUR^{1,*}

¹Department of Chemical Technology, Iranian Research Organization for Science and Technology (IROST), Tehran, 3313193685, Iran

*Corresponding author e-mail: Habibpour@irost.ir, marandjbar@irost.ir

Received date:

11 March 2023

Revised date

1 June 2023

Accepted date:

13 June 2023

Keywords:

Zeolite imidazolate framework;
Adsorption;
Heavy metals;
Optimization;
Response surface methodology

Abstract

A Zeolitic imidazolate framework-8 (ZIF-8) was synthesized by the solvothermal method of zinc nitrate hexahydrate and 2-methylimidazole in DMF to remove Cd(II), Ni(II), and Pb(II) ions from aqueous solutions. The synthesized ZIF-8 was distinguished by XRD, FT-IR, BET, SEM, EDX, TEM methods. Several significant variables were optimized with response surface methodology (RSM) to obtain the highest removal of metal ions. According to the achieved results, the aqueous solution pH values of 6.5, 6.5, and 6.0, ZIF-8 dosages of 0.05, 0.06, and 0.05 g.L⁻¹, and metal ions initial concentrations of 50, 60, and 60 mg.L⁻¹ were chosen as the optimum amount of these variables for Cd(II), Ni(II), and Pb(II) ions adsorption from solution, respectively. The equilibrium time for metal ions adsorption was found at 50 min. Three-dimensional plots demonstrate relationships between the metal ion uptakes with the paired factors, which illustrate the behavior of the sorption system in a batch process. Based on the experimental results and model parameters, maximum adsorption efficiencies were achieved 89.76, 72 and 68.43% for Cd(II), Ni(II) and Pb(II), respectively. It can be suggested that the synthesized ZIF-8 has excellent potential as an effective adsorbent and used for heavy metal sorption from water environment.

1. Introduction

The environment has been heavily polluted by contaminating water resources due to the rapid growth of industry and agriculture. The pollution of water resources from the indiscriminate disposal of heavy metals has been causing worldwide concern for many decades and has garnered increasing attention. Heavy metals are among the water pollution sources that are highly toxic to human health [1-3]. Therefore, they must be removed from wastewater to protect public health. Although many heavy metals are critical to biological systems [4], exceeding the provisional maximum tolerable daily intake can cause toxicity for ecological, evolutionary, nutritional and environmental reasons [5]. Heavy metal ions, such as Cd(II), Ni(II), Pb(II), Cr(VI), As (III), Cu(II), Hg(II), etc. are highly water soluble, toxic and have the ability to migrate that must be removed from wastewater before they are released into the environment [6,7]. Several conventional methods have been developed to remove them from wastewater as well as in water purification [8]: adsorption, ion-exchange, solvent extraction, chemical precipitation, membrane filtration, bio-adsorption, electrodialysis, coagulation and flocculation, flotation, and electrochemical treatment. Among these methods, adsorption is widely applied for its benefits, such as low cost, high efficiency, simple design, and selectivity for removing heavy metals at very low concentrations. Zeolitic imidazolate frameworks (ZIFs), as a member of the crystalline porous frameworks coordinated by Zn²⁺ and

2-methylimidazole, are widely used in gas separation, heterogeneous catalysis, separation of organic chemicals, and adsorption; it has advantages such as being highly porous, having large pore volume and high specific surface area, and exceptional chemical and thermal stabilities [9]. Therefore, ZIFs can be considered a promising candidate for selective adsorption and wastewater treatment. In recent years, metal-organic frameworks have been employed extensively as a new adsorbent for removing heavy metal from aqueous solutions. The adsorption mechanism for metal ions includes ion exchange, coordination reaction, and hybrid of them. For metal ions (Mⁿ⁺) with the same atomic number as zinc, Zn²⁺ in ZIF-8 can be easily replaced by Mⁿ⁺. If the valence electron layer structure of Zn²⁺ is more stable than that of Mⁿ⁺, the chemical coordination ability of Mⁿ⁺ is stronger than that of Zn²⁺, and as a result, the coordination reaction will occur between Mn²⁺ and the nitrogen atom on 2-methylimidazole [10]. Niknam Shahrak *et al.* [11] synthesized ZIF-8 by a precipitation method and used it to remove chromium (VI) ions from an aqueous solution. They stated that the neutral environment (pH=7) was more favorable for Cr(VI) removal by ZIF-8 microcrystals. Wang *et al.* [12] synthesized ZIF-8 by a precipitation method used in removing copper (II) ions from an aqueous solution. They indicated that ZIF-8 nanocrystals demonstrated an unexpectedly high adsorption capacity of Cu²⁺ and high removal efficiency for both high and low concentrations of Cu²⁺ from water. Tanihara *et al.* [13] synthesized monodisperse ZIF-8 fine particles by a precipitation method in the presence of

a nonionic surfactant and used it to remove Pb^{2+} and Cu^{2+} ions. According to their results, the Pb^{2+} and Cu^{2+} removal occurred through the adsorption mechanism and ion-exchange phenomenon, respectively. ZIF-8 is one of the most stable structures among MOF materials in aqueous solutions, which can be prepared through different synthesis routes, such as solvo-hydro thermals [14,15], microwave-assisted [16], sonochemical [17], mechanochemical [18], dry-gel [19], and microfluidic [20]. Among them, the solvo-hydro thermal methods are preferred due to the good yields and purity of the produced ZIFs. It was necessary to consider and optimize several variables that could affect the adsorption process to obtain the highest adsorption efficiency. In most of the previous studies, optimizing effective parameters involved repetitive changes of one independent variable while maintaining all others at fixed levels, which was time-consuming and expensive. This method of optimizing could not determine the magnitudes of interactions among the process variables, but this study employed Response Surface Methodology (RSM) based on central composite design (CCD) technique to optimize the adsorption of heavy metal ions from aqueous solution onto ZIF-8. CCD and RSM were applied as experimental strategies for modeling and optimizing the values of some effective parameters on the removal of heavy metals from wastewater. Furthermore, the influence of the interactions between the parameters was well identified; the time and the number of tests were also optimized using the experimental design.

In the present study, ZIF-8 was synthesized with solvothermal method using zinc nitrate as the metal source and 2-methylimidazole as the organic ligand in the presence of the dimethylformamide (DMF) as solvent and used for the adsorption of Cd(II), Ni(II), and Pb(II) ions from aqueous solution under batch conditions. As a result, synthesized ZIF-8 demonstrate the highest removal efficiency of Cd^{2+} over other heavy metal ions.

2. Experimental

2.1 Materials and Measurements

All chemicals and reagents with analytical grade obtained from the Sigma-Aldrich and Merck companies and were used as received without any further purification. Many tests were applied to characterize the synthesized ZIF-8 comprehensively. The functional groups of the synthesized materials were investigated using an FT-IR spectrometer (AVATAR, Thermo Nicolet Co., USA). FE-SEM analyze was used to observe the morphological structure of the prepared ZIF-8. EDX elemental analysis was carried out with a TESCAN VEGA3 microscope at an accelerating voltage of 30 kV. The composition or amount of nanoparticles near and at the surface was estimated using EDX. The XRD measurement was done using a Philips PW1730 X-ray diffractometer (Cu $K\alpha$, 40 kV, 30 Ma, $\lambda = 1.54056 \text{ \AA}$) to recognize the crystal structure of the synthesized ZIF-8. BET analysis (Belsorp mini II, Microtrac Bel Corp Company, Japan) was used to determine the specific surface area and pore size distribution measurement through N_2 adsorption/desorption at 77 K. The TEM images were obtained using a Philips CM-10 TEM microscope (100 kV) to determine the particle size, shape, and distribution. This analysis was performed under argon atmosphere with a heating rate of $10^\circ\text{C min}^{-1}$. An atomic absorption spectrometer (AAS, VARIAN AA240, USA)

was applied to determine the concentration of heavy metal ions after adsorption on synthesized ZIF-8.

2.2 Statistical software

Essential Regression and Experimental Design for chemists and Engineers (EREGRESS), MS Excel Add-in software, was used to design the experiments and model and analyze the results.

2.3 Synthesis of ZIF-8

The ZIF-8 was synthesized following a solvothermal method in the literature procedure [21]. Briefly, 1.88 g zinc nitrate hexahydrate was dissolved in 15 mL of N,N-dimethylformamide (DMF) as solvent. In the following, this solution was added into a Teflon-lined autoclave containing 2-methylimidazole solution (0.43 g 2-methylimidazole in 15 ml DMF). Afterwards, the autoclave heated at 140°C for 24 h to produce the white crystals of ZIF-8 and then cooled at a rate of $0.4^\circ\text{C min}^{-1}$ to room temperature. The crystals were collected by filtration, washed with chloroform, and dried in the air. Before adsorption process, the residual solvents were dried under vacuum at 200°C for at least 6 h, yielding 0.20 g of crystals.

2.4 Batch adsorption experiments

The adsorption of lead, cadmium, and nickel on ZIF-8 was studied using the batch process. For each experimental run, a 100 mL aqueous solution of the known concentration of Pb(II), Cd(II), and Ni(II) was poured into a conical flask containing a certain amount of adsorbent. These flasks were agitated with a temperature-controlled shaker at a constant rate of 300 rpm.

The effect of the initial concentration of heavy metal ions, pH of solution, adsorbent dosage, and contact time on the adsorption performance of ZIF-8 was investigated. $Pb(NO_3)_2 \cdot 4H_2O$, $Cd(NO_3)_2 \cdot 4H_2O$, and $Ni(NO_3)_2 \cdot 4H_2O$ were used as the sources of Pb(II), Cd(II), and Ni(II), respectively. In this process, the initial metal ion concentration varied over a range of $10 \text{ mg}\cdot\text{L}^{-1}$ to $100 \text{ mg}\cdot\text{L}^{-1}$. The effect of pH on the adsorption was investigated in a pH range of 3.0 to 9.0 and the effect of adsorbent dosage was studied by varying the dosage from $0.01 \text{ g}\cdot\text{L}^{-1}$ to $0.05 \text{ g}\cdot\text{L}^{-1}$. The samples were taken at 5-120 min to determine optimal contact time. Then, the supernatants were centrifuged at 300 rpm for 10 min, and the filtrate was analyzed for Pb(II), Cd(II), and Ni(II) concentration by AAS. The removal efficiency (% adsorption) was calculated using the following relation (Equation. 1).

$$\text{Removal efficiency (\%)} = \frac{C_0 - C_e}{C_0} \times 100 \quad (1)$$

Where C_0 and C_e represent the initial and equilibrium metal ions concentrations (mg/L) in the solution, respectively.

2.5 Central composite design (CCD)

Central composite design (CCD) was employed to investigate and optimize the experimental variables in the adsorption of Cd(II), Ni(II), and Pb(II). Four independent factors, including the initial

concentration of metal ion (F1), pH (F2), adsorbent dosage (F3), and contact time (F4), were studied at five levels with four repetitions at the central point using a circumscribed CCD. High (coded value: +1.607) and low (coded value: -1.607) set points were selected for each of the four studied factors, as shown in Tables 1(a-c) for Cd(II), Ni(II), and Pb(II), respectively. Also, Tables 2(a-c) show the coded and real values of the designed experiments based on CCD methodology achieved using EREGRESS software for Cd(II), Ni(II), and Pb(II), respectively.

Polynomial equations and response surfaces for a particular response were created using EREGRESS. For an experimental design with four factors, the linear, quadratic, and cross-terms models can be expressed as Equation 2:

$$\begin{aligned} \text{Response} = & b_0 + (b_1 \times F_1) + (b_2 \times F_2) + (b_3 \times F_3) + (b_4 \times F_4) + \\ & (b_5 \times F_1 \times F_1) + (b_6 \times F_2 \times F_2) + (b_7 \times F_3 \times F_3) + (b_8 \times F_4 \times F_4) + \\ & (b_9 \times F_1 \times F_2) + (b_{10} \times F_1 \times F_3) + (b_{11} \times F_1 \times F_4) + (b_{12} \times F_2 \times F_3) + \\ & (b_{13} \times F_2 \times F_4) + (b_{14} \times F_3 \times F_4) \end{aligned} \quad (2)$$

Where F1-F4 are the variable parameters and b0-b14 are the coefficient values obtained through multiple linear regression (MLR) using EREGRESS. The response surface plots were achieved through a statistical process that described the design and the modeled CCD data. The response surface methodologies graphically demonstrated the relationships between the parameters and responses, providing a way to obtain an optimum [22-25]. The statistical significance of the predicted models was appraised by the analysis of variance (ANOVA) and least-squares techniques. ANOVA determines which factors significantly affect the studied response variables using Fisher's

statistical test (F-test). The significance and the magnitude of the estimated coefficients of each variable and all their possible interactions on the response variables were determined. Such coefficients for each variable represented the improvement in the response; the variable setting was expected to change from low to high. Effects with less than 95% of significance (with a p-value higher than 0.05) were discarded and pooled into the error term. A new analysis of variance was performed for the reduced model [22]. Note that the p-value represented a decreasing index of the reliability of a result. Replicates (n=4) of the central points were performed to estimate the experimental error.

3. Results and discussion

3.1 Characterization of ZIF-8

3.1.1 Field emission Scanning electron microscopy (FE-SEM)

FE-SEM is a powerful instrument for investigating the size of the materials and revealing important information on surface morphology. As seen in Figure 1, the octahedral crystals of the synthesized ZIF-8 were visible and had some cavities in their structure capable of uptaking metal ions [26,27]. Since the synthesized ZIF-8 has the highest efficiency in adsorbing Cd(II), only the FE-SEM images of the ZIF-8 after Cd(II) adsorption in optimal conditions are presented in Figure 2. After adsorption, the octahedral crystal structure of the ZIF-8 is conserved. Although the amount of cavities in the structure that have the ability to uptaking the metal ions has decreased significantly.

Table 1(a). The variables and values used for a central composite design for Cd(II).

Coded factor levels					
Variable name	-1.607(low)	- 0.8	0	+0.8	+1.607(high)
F1 initial concentration (mg.L ⁻¹)	10	22.5	35	47.5	60
F2 pH	3	4.75	6.5	8.24	10
F3 adsorbent dosage (g.L ⁻¹)	0.01	0.023	0.035	0.047	0.06
F4 contact time (min)	5	33.87	62.5	91.125	120

Table 1(b). The variables and values used for a central composite design for Ni(II).

Coded factor levels					
Variable name	-1.607(low)	- 0.8	0	+0.8	+1.607(high)
F1 initial concentration (mg.L ⁻¹)	5	20	35	50	65
F2 pH	4	5	6	7	8
F3 adsorbent dosage (g.L ⁻¹)	0.01	0.025	0.04	0.055	0.07
F4 contact time (min)	5	18.75	32.5	46.25	60

Table 1(c). The variables and values used for a central composite design for Pb(II).

Coded factor levels					
Variable name	-1.607(low)	- 0.8	0	+0.8	+1.607(high)
F1 initial concentration (mg.L ⁻¹)	10	22.5	35	47.5	60
F2 pH	4	5	6	7	8
F3 adsorbent dosage (g.L ⁻¹)	0.01	0.023	0.035	0.047	0.06
F4 contact time (min)	5	26.25	47.5	68.75	90

Table 2(a). List of CCD experiments for model optimization (coded values) in the adsorption of Cd(II).

Factor levels					
Design points	F1	F2	F3	F4	Response (%)
1	-0.8	0.8	-0.8	0.8	63.91
2	0.8	0.8	-0.8	0.8	76.00
3	-0.8	0.8	-0.8	-0.8	55.00
4	0.8	-0.8	-0.8	0.8	71.40
5	-0.8	-0.8	0.8	-0.8	63.50
6	-0.8	0.8	0.8	0.8	76.23
7 ^(cp)	0.0	0.0	0.0	0.0	83.12
8	-0.8	-0.8	-0.8	0.8	58.98
9	0.0	1.607	0.0	0.0	73.00
10	0.0	0.0	0.0	-1.607	59.34
11	0.0	0.0	0.0	1.607	86.00
12 ^(cp)	0.0	0.0	0.0	0.0	82.00
13	0.8	0.8	-0.8	-0.8	71.34
14 ^(cp)	0.0	0.0	0.0	0.0	82.00
15 ^(cp)	0.0	0.0	0.0	0.0	82.50
16	-0.8	-0.8	0.8	0.8	75.23
17	0.8	0.8	0.8	-0.8	81.65
18	0.8	-0.8	0.8	0.8	82.00
19	0.0	0.0	-1.607	0.0	55.43
20	0.8	0.8	0.8	0.8	89.76
21	-1.607	0.0	0.0	0.0	58.54
22	-0.8	0.8	0.8	-0.8	70.65
23	0.0	-1.607	0.0	0.0	54.65
24	1.607	0.0	0.0	0.0	86.30
25	0.0	0.0	1.607	0.0	87.00
26	-0.8	-0.8	-0.8	-0.8	47.80
27	0.8	-0.8	-0.8	-0.8	58.00
28	0.8	-0.8	0.8	-0.8	72.40

^(cp) indicates four repetitions of center points

Table 2(b). List of CCD experiments for model optimization (coded values) in the adsorption of Ni(II).

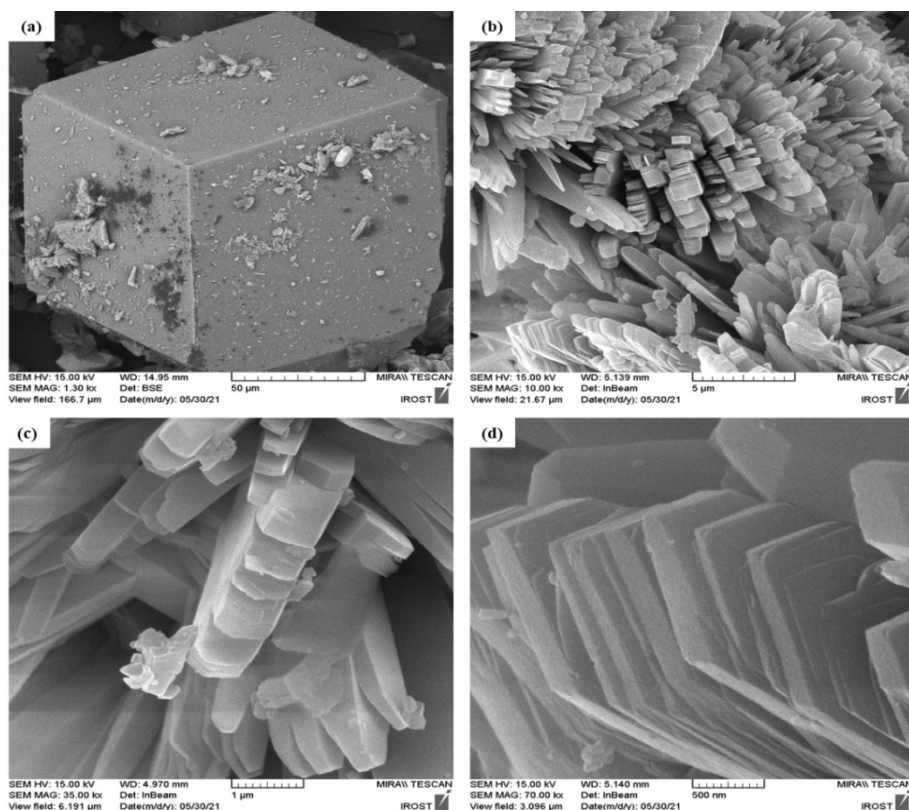
Factor levels					
Design points	F1	F2	F3	F4	Response (%)
1	0.0	0.0	-1.607	0.0	34.45
2	0.8	0.8	0.8	-0.8	56.52
3	0.8	0.8	0.8	0.8	72.32
4	0.8	0.8	-0.8	0.8	58.02
5	0.0	1.607	0.0	0.0	38.23
6	-0.8	-0.8	-0.8	0.8	40.04
7	0.8	-0.8	-0.8	-0.8	42.26
8	0.0	0.0	0.0	1.607	56.23
9 ^(cp)	0.0	0.0	0.0	0.0	52.45
10	-1.607	0.0	0.0	0.0	42.65
11	-0.8	0.8	0.8	0.8	58.34
12 ^(cp)	0.0	0.0	0.0	0.0	52.65
13	-0.8	0.8	-0.8	-0.8	35.21
14	0.0	-1.607	0.0	0.0	35.23
15	-0.8	-0.8	-0.8	-0.8	30.14
16	-0.8	-0.8	0.8	0.8	53.07
17	0.8	-0.8	-0.8	0.8	55.74
18	0.8	0.8	-0.8	-0.8	49.43
19	-0.8	-0.8	0.8	-0.8	54.84
20	1.607	0.0	0.0	0.0	72.00
21 ^(cp)	0.0	0.0	0.0	0.0	52.46
22 ^(cp)	0.0	0.0	0.0	0.0	52.37
23	-0.8	0.8	0.8	-0.8	47.34
24	0.8	0.8	0.8	-0.8	62.54
25	0.8	-0.8	0.8	0.8	62.28
26	0.0	0.0	1.607	0.0	58.34
27	0.0	0.0	0.0	-1.607	37.24
28	-0.8	0.8	-0.8	0.8	45.24

^(cp) indicates four repetitions of center points

Table 2(c). List of CCD experiments for model optimization (coded values) in the adsorption of Pb(II).

Factor levels					
Design points	F1	F2	F3	F4	Response (%)
1	0.8	0.8	-0.8	0.8	55.34
2	0.8	-0.8	0.8	0.8	64.34
3	0.8	-0.8	0.8	-0.8	52.45
4	0.8	0.8	0.8	-0.8	56.45
5 ^(cp)	0.0	0.0	0.0	0.0	59.33
6	0.8	0.8	-0.8	-0.8	45.61
7	-0.8	0.8	-0.8	0.8	48.16
8	0.0	1.607	0.0	0.0	49.43
9	-0.8	0.8	0.8	0.8	59.45
10	-0.8	0.8	0.8	-0.8	46.53
11	0.0	-1.607	0.0	0.0	35.37
12	0.0	0.0	1.607	0.0	68.43
13	0.8	0.8	0.8	0.8	66.89
14 ^(cp)	0.0	0.0	0.0	0.0	60.20
15	0.8	-0.8	-0.8	0.8	49.21
16	0.0	0.0	0.0	1.607	65.47
17	-1.607	0.0	0.0	0.0	42.36
18	0.0	0.0	-1.607	0.0	38.68
19 ^(cp)	0.0	0.0	0.0	0.0	59.21
20 ^(cp)	0.0	0.0	0.0	0.0	57.21
21	0.0	0.0	0.0	-1.607	38.00
22	1.607	0.0	0.0	0.0	64.43
23	-0.8	-0.8	0.8	-0.8	42.78
24	-0.8	-0.8	-0.8	0.8	47.45
25	-0.8	-0.8	-0.8	-0.8	39.13
26	-0.8	-0.8	0.8	0.8	54.37
27	0.8	-0.8	-0.8	-0.8	44.31
28	-0.8	0.8	-0.8	-0.8	39.43

^(cp) indicates four repetitions of center points

**Figure 1.** FE-SEM images of synthesized ZIF-8 at different magnification scale.

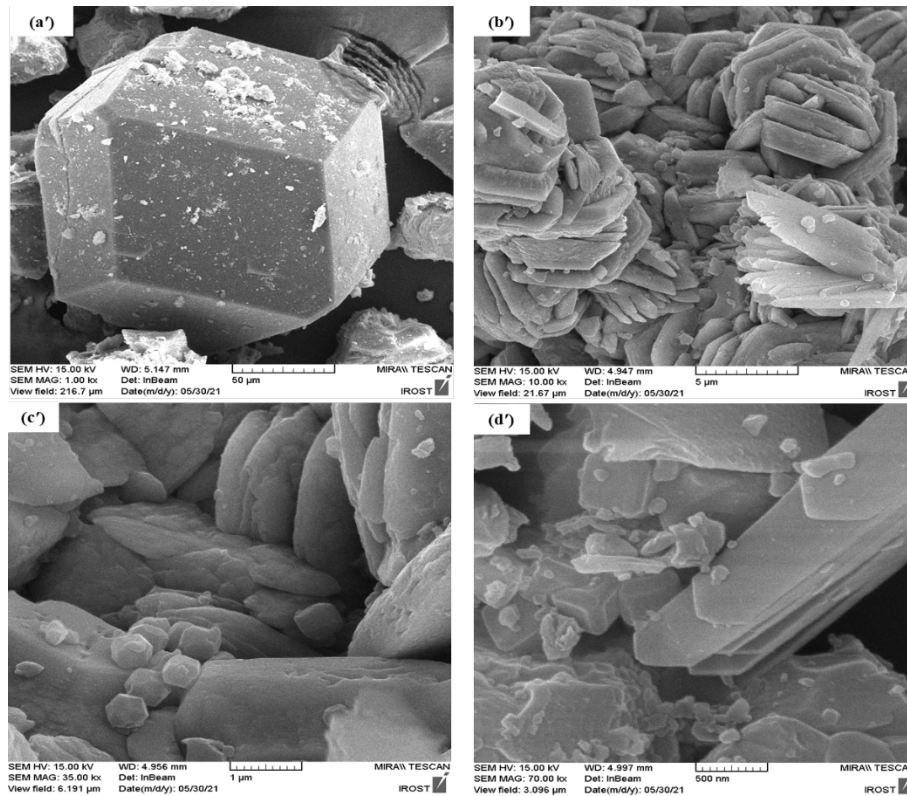


Figure 2. FE-SEM images of synthesized ZIF-8 after adsorption of Cd(II) at different magnification scale.

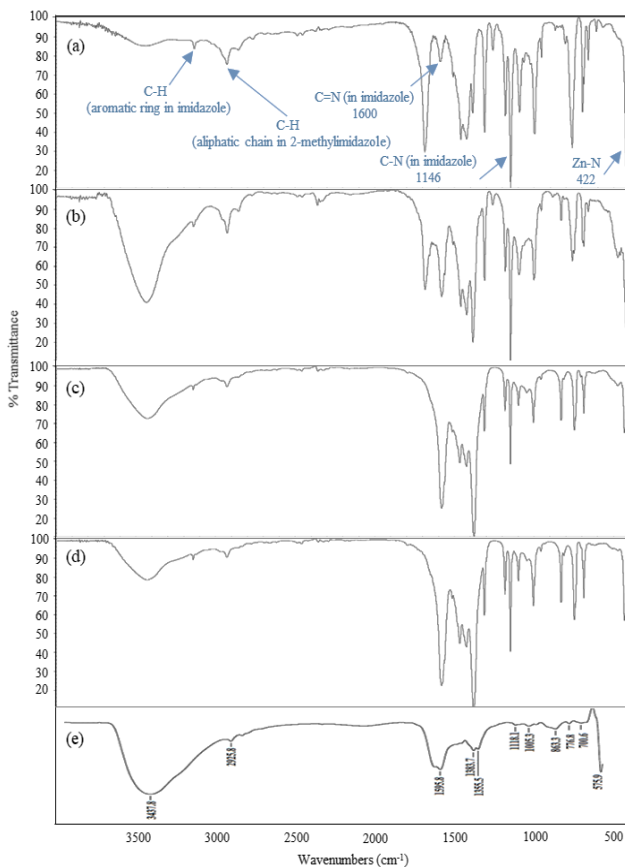


Figure 3. FTIR spectra of ZIF-8 (a) before adsorption (b) after adsorption of Cd(II) (c) after adsorption of pb(II) (d) ZIF-8 after adsorption of Ni(II), and (e) 2-methyleimidazole.

3.1.2 Fourier transform infrared spectroscopy (FT-IR)

The FTIR spectra of ZIF-8 before and after adsorbing ion metals are shown in Figure 3(a-d); the FT-IR spectrum for the synthesized ZIF-8 is demonstrated in the wavenumber range of 500 cm^{-1} to 4000 cm^{-1} . As seen in Figure 3(a), the bands at 3130 cm^{-1} and 2920 cm^{-1} were due to the stretching vibrations of C-H bonds in the aromatic ring in the imidazole and aliphatic chain in 2-methylimidazole, respectively. The band at 1600 cm^{-1} was attributed to the stretching mode of C=N bonding. The bands at 600 cm^{-1} to 1500 cm^{-1} were related to the stretching and bending modes of the imidazole ring. Finally, the adsorption peak at 422 cm^{-1} showed the Zn-N bond stretching when the zinc atoms in ZIF-8 connected to the nitrogen atoms of the 2-methylimidazole linker during ZIF-8 synthesis. The presence of an imidazole group and Zn-N interaction was confirmed by the Fourier-transform infrared spectra of ZIF-8, which confirmed that the synthesis of ZIF-8 crystals was in good agreement with the reported ones [28,29]. The FTIR spectra of ZIF-8 before and after ion metals adsorbing were different. As shown in Figures 3(b-d), after the interaction between the ion metal and adsorbent, two new peaks were observed at 500 cm^{-1} and 1380 cm^{-1} , which demonstrated that M (M=Cd(II), Ni(II) and Pb(II)) were coordinated with the nitrogen atom on 2-methylimidazole. Meanwhile, the peaks in the range of 2800 cm^{-1} to 3200 cm^{-1} were weakened. Regarding the preservation of the ZIF-8 framework, it could be said that adsorption was the main process involved in these three metal ions removal. In addition to adsorption, ion exchange also occurred for Ni(II), and the appearance of a wide peak in the region of 3300 cm^{-1} to 3700 cm^{-1} attributable to zinc oxide confirmed this. The amount of ion exchange for the Cd(II) and Pb(II) ions occurred with less intensity than Ni(II).

3.1.3 X-ray diffraction XRD

The XRD pattern of the crystalline structure of the synthesized ZIF-8 is presented in Figure 4. The stronger peaks at $2\theta = 7.4, 10.6, 13.1, 15.1, 16.6,$ and 18.2 correspond to planes 110, 200, 211, 220, 310, and 222, respectively, indicating high crystallinity of the prepared ZIF-8 [30, 31].

3.1.4 Brunauer-Emmet-Teller (BET)

Figure 5 and Table 3, present the N_2 adsorption/desorption isotherms and pore characteristics of the synthesized ZIF-8. A Type I isotherm indicated the microporosity nature of the synthesized ZIF-8. At low values of P/P_0 , the adsorption rate of N_2 gas on the surface of the synthesized ZIF-8 was very high and gradually decreased due to the filling of the pores. Very small steps at higher pressure with a hysteresis loop were representative of the existence of large mesopores between the adjacent ZIF-8 crystalline particles. The measured BET and Langmuir surface areas of the synthesized ZIF-8 were $703.4 \text{ m}^2 \cdot \text{g}^{-1}$ and $827.3 \text{ m}^2 \cdot \text{g}^{-1}$, respectively, with a mean pore diameter of 1.2 nm and total pore volume of $0.34 \text{ cm}^3 \cdot \text{g}^{-1}$, which were in good agreement with another reported isotherm [32,33].

3.1.5 Energy Dispersive Spectroscopy EDS

The EDS analysis of the synthesized ZIF-8 is shown in Figure 6. As can be seen, C, N, and Zn elements were present in ZIF-8. Also, the elemental mapping analysis confirmed the EDXS data and homogeneous dispersion of C, N, and Zn elements near and at the surface of the adsorbent. The N atoms found in the structure of the synthesized ZIF-8 came from the 2-methylimidazole ligand [34-36]. The EDS analysis of the ZIF-8 after Cd(II) adsorption also shows

the uniform distribution of C, N, and Zn elements and confirms the adsorption of cadmium (Figure 7).

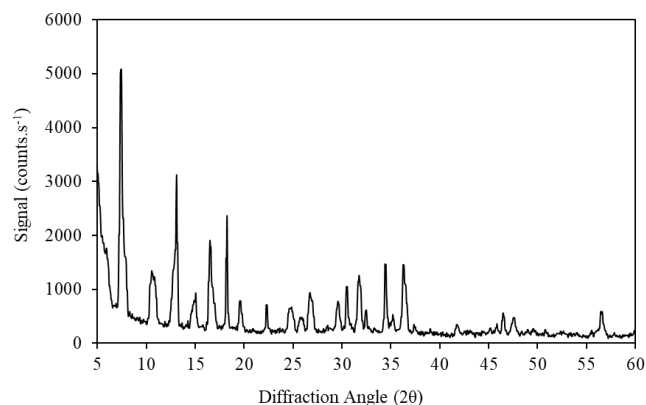


Figure 4. XRD pattern of the synthesized ZIF-8.

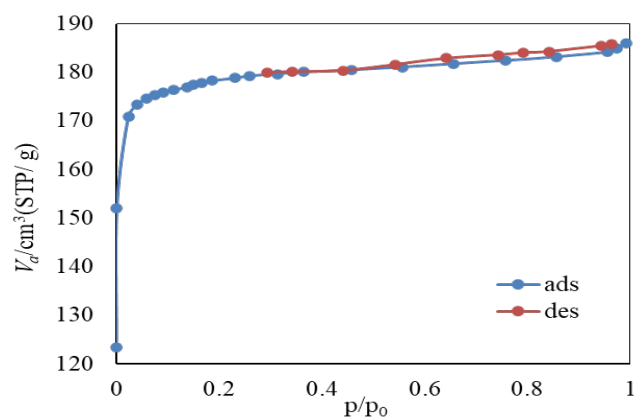


Figure 5. Nitrogen adsorption/desorption isotherm of synthesized ZIF-8..

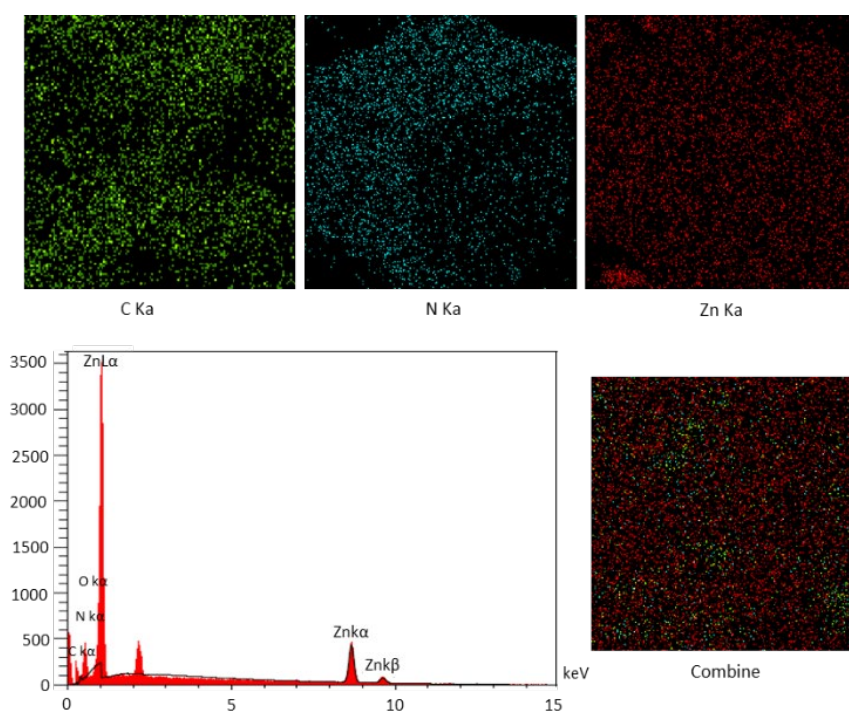


Figure 6. Energy dispersive spectra and elemental mapping of C, Zn, and N for ZIF-8.

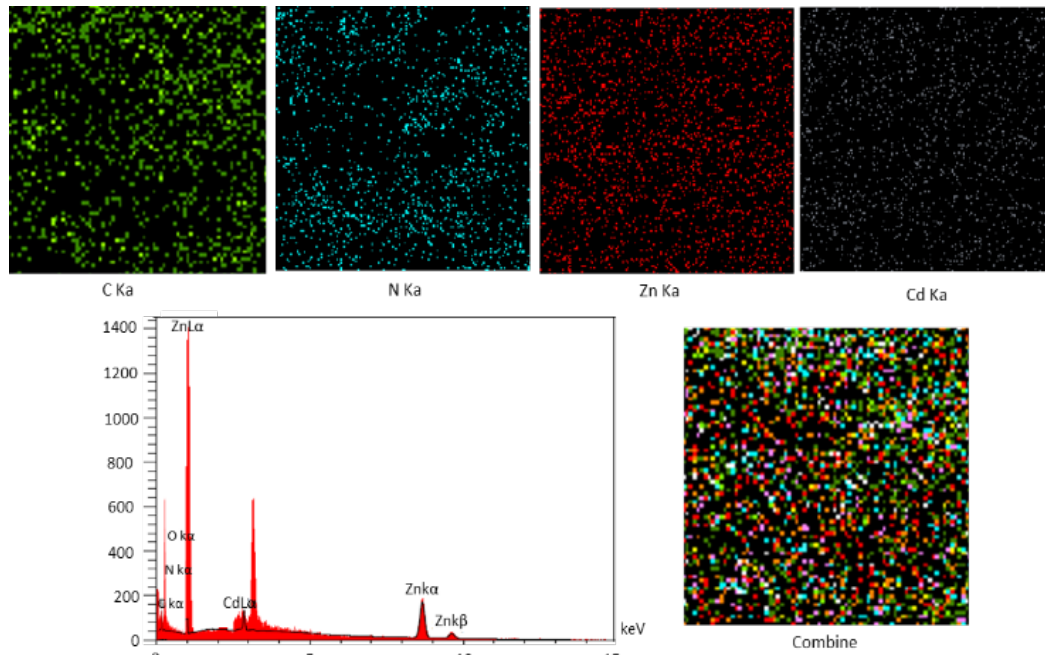


Figure 7. Energy dispersive spectra and elemental mapping of C, Zn, N, and Cd for ZIF-8 after adsorption of Cd(II).

Table 3. The results obtained by BET analysis of ZIF-8.

BET surface area ($\text{m}^2\cdot\text{g}^{-1}$)	Langmuir surface area ($\text{m}^2\cdot\text{g}^{-1}$)	Mean pore diameter (nm)	Total pore volume ($\text{cm}^3\cdot\text{g}^{-1}$)
703.41	827.38	1.2513	0.3428

3.1.6 Transmission electron microscopy TEM

In order to provide an image of the bulk synthesized ZIF-8 and also show its 3-dimensional shape, the structure of the synthesized ZIF-8 was characterized by TEM [37,38]. The images are presented in Figure 8, showing particles with nano size and sharp hexagonal faces. The particles were 12 nm to 30 nm in diameter, which agreed with the FE-SEM observation (Figure 1).

3.2 Experimental design

The adsorption of the samples was collected as a response to optimize four independent factors, namely the initial concentration of the metal ion (F1), pH (F2), adsorbent dosage (F3), and contact time (F4). Tables 1-2, show the levels of coded and real experimental variables that were tested. In addition, Table 2 presents the corresponding response of each run. The goals of the CCD strategy included the following: (i) study the effect of pH, initial concentration of metal ions, adsorbent dosage, and contact time on the adsorption of Cd(II), Ni(II), and Pb(II); (ii) identify the variables that had a higher impact on the adsorption procedure; (iii) give insight into the robustness of the technique close to the optimum conditions; and (iv) show the interactions between the variables [39,40]. A full quadratic model, including all terms of Equation (2), was used to find the critical factors and build a model to optimize the method. To achieve a simple and yet realistic model, the insignificant terms ($p > 0.05$) were eliminated from the model through the ‘backward elimination’ process. Using all 15 terms of Equation 2, the constructed model showed a relatively good fit. A

regression coefficient (R^2) for calibration close to one was obtained for this model. Some of these 15 regression variables were insignificant or of low significance and were eliminated from the model. In statistical modeling, R^2 always decreases when a regression variable is eliminated from a regression model, and the adjusted R-squared (R^2_{adj}) is usually selected by considering the number of regression variables. Also, the predicted R-squared (R^2_{pred}), which shows the model’s predictive power, is chosen for the same reason. This parameter is approximated using the predicted residual error sum of squares (PRESS) calculated from the residuals that is based on a regression model with one data point eliminated. So, the three coefficients of R^2 , R^2_{adj} , and R^2_{pred} together provide a quick impression of the overall fit of the model and the predictive power based on the one data point eliminated. In an appropriate model, these parameters should not be too different from each other. However, every data point is likely influential for the small data sets. A high value for R^2_{pred} cannot be expected in these cases. By eliminating the insignificant parameters from Equation 2, the final amount of R^2 decreased to 0.983, 0.959, and 0.939 for Cd(II), Ni(II), and Pb(II), respectively. But R^2_{adj} : R^2_{pred} increased to nearly 0.973:0.935, 0.945:0.862, and 0.914:0.791 for Cd(II), Ni(II), and Pb(II), respectively. The obtained reduced models using the significant linear, quadratic, and interaction parameters are shown in Tables 4-6 for Cd(II), Ni(II), and Pb(II), respectively. It should be mentioned that the regression equations were achieved using the uncoded values of the parameters. There were no significant differences between the R^2 values, which revealed that the experimental data exhibited a good fit with the third-order polynomial equations.

3.3 Response surface and selection of optimum conditions

In order to obtain insight into the effect of each variable, three-dimensional (3D) plots for the predicted responses were prepared based on the model function to analyze the change of the response surface. Figure 9-11, show some of the response surface plots that revealed the relationship between two variables and the adsorption of the samples, while two other variables were kept at medium levels. As shown in the figures, there was a non-linear relation between the response and variables F1–F4 because the surface plots of the response

were curves. Several linear, squared, and statistically significant interaction parameters are shown in Table 4-6; the selection of optimum conditions for the method was possible using the response surface plots. The plots showed the interaction between the mentioned factors when the remaining factors were fixed at a central point. The results showed a pronounced adsorption dependency on all of the investigated experimental factors, the initial concentration of metal ion (F1), pH (F2), adsorbent dosage (F3), and contact time (F4), which significantly affected the adsorption modeling by both linear and quadratic variables.

Table 4. Some characteristics of the constructed models to obtain an optimized system for adsorption of Cd(II) on ZIF-8.

Regression equation	Coefficients	values	P values
Adsorption = $b_0 + b_1 \cdot \text{Conc} + b_2 \cdot \text{pH} + b_3 \cdot \text{Dosage} + b_4 \cdot \text{Time} + b_5 \cdot \text{Conc} \cdot \text{Conc} + b_6 \cdot \text{Conc} \cdot \text{pH} + b_7 \cdot \text{pH} \cdot \text{pH} + b_8 \cdot \text{pH} \cdot \text{Time} + b_9 \cdot \text{Dosage} \cdot \text{Dosage} + b_{10} \cdot \text{Time} \cdot \text{Time}$	b0	-99.82	5.7007E-08
	b1	1.366	1.9453E-05
	b2	22.18	2.9725E-09
	b3	1858.2	1.1902E-08
	b4	0.712	3.5545E-07
	b5	-0.01642	6.6247E-06
	b6	0.04191	0.07931
	b7	-1.539	1.3790E-09
	b8	-0.02317	0.02970
	b9	-18348.7	1.6311E-06
b10	-0.00303	8.9460E-06	
R	0.992		
R ²	0.983		
R ² adj	0.973		
R ² pred	0.935		
No. points	28		

Table 5. Some characteristics of the constructed models to obtain optimized system for an adsorption of Ni(II).

Regression equation	Coefficients	values	P values	
Adsorption = $b_0 + b_1 \cdot \text{pH} + b_2 \cdot \text{Dosage} + b_3 \cdot \text{Time} + b_4 \cdot \text{Conc} \cdot \text{Conc} + b_5 \cdot \text{pH} \cdot \text{pH} + b_6 \cdot \text{Dosage} \cdot \text{Dosage} + b_7 \cdot \text{Time} \cdot \text{Time}$	b0	-130.41	2.13402E-06	
	b1	42.93	8.91296E-07	
	b2	749.07	0.000628	
	b3	0.666	0.00139	
	b4	0.00670	1.5817E-11	
	b5	-3.391	1.81637E-06	
	b6	-4332.6	0.07066	
	b7	-0.00471	0.09671	
	R	0.979		
	R ²	0.959		
R ² adjusted	0.945			
R ² for prediction	0.862			
No. points	28			

Table 6. Some characteristics of the constructed models to obtain an optimized system for adsorption of Pb(II).

Regression equation	Coefficients	values	P values
Adsorption = $b_0 + b_1 \cdot \text{Conc} + b_2 \cdot \text{pH} + b_3 \cdot \text{Dosage} + b_4 \cdot \text{Time} + b_5 \cdot \text{Conc} \cdot \text{Conc} + b_6 \cdot \text{pH} \cdot \text{pH} + b_7 \cdot \text{Dosage} \cdot \text{Dosage} + b_8 \cdot \text{Time} \cdot \text{Time}$	b0	-169.40	1.64492E-06
	b1	0.929	0.00258
	b2	50.98	7.89988E-07
	b3	1020.2	0.00119
	b4	0.627	9.1972E-05
	b5	-0.00844	0.03723
	b6	-4.068	1.38054E-06
	b7	-8188.0	0.04270
	b8	-0.00384	0.00832
	R	0.969	
R ²	0.939		
R ² adjusted	0.914		
R ² for prediction	0.791		
No. points	28		

Table 7. Range of optimum conditions obtained by response surface modeling for metal ions removal and their corresponding selected values.

Metal ion	Condition	Concentration (mg·L ⁻¹)	pH	Dosage of ZIF-8 (g·L ⁻¹)	Contact time (min)
Cd(II)	Optimum values	45-55	6.1-6.8	0.045-0.055	55-60
	Selected values	50	6.5	0.05	50
Ni(II)	Optimum values	60-65	6-6.5	0.06-0.07	45-60
	Selected values	60	6.5	0.06	50
Pb(II)	Optimum values	50-60	5.8-6.2	0.04-0.06	50-90
	Selected values	60	6	0.05	50

3.3.1 Effect of pH

The pH of solution is one of the most important factors in the adsorption of metal ions. The effect of pH on the adsorption of Cd(II), Ni(II) and Pb(II) onto synthesized ZIF-8 was investigated at the pH range of 3 to 9 (Figure 9-11). In these figures, the adsorption efficiency dramatically increased by increasing the pH; it reached a maximum at pH 6 to 6.5 and then decreased. Based on the results, ion adsorption increased at pH 2 to 6 due to an increase in the positive charge density on the surface sites; thus, electrostatic repulsion occurred between the ions and the edge group with a positive charge on the surface. Also, with the increase of a pH higher than 5.5, the competing effect

of H⁺ ions decreased, and the positively charged metal ions connected to the free binding sites. Hence, the metal ion uptake increased on the surface of the adsorbent with the increase in pH [41,42]. At pH values higher than 7, metal precipitation occurred, and the adsorbent capacity decreased with the accumulation of metal ions [43,44]. Based on the results and shown in Table 7, the range of pH from 6.1 to 6.8, 6 to 6.5, and 5.8 to 6.2 were selected as the optimum pH values for further studies of Cd(II), Ni(II), and Pb(II) metal ion removal by synthesized ZIF-8, respectively. According to these results, the pH values of 6.5, 6.5, and 6.0 were chosen as the optimum amount of solution pH for Cd(II), Ni(II), and Pb(II) metal ion adsorption from solution, respectively.

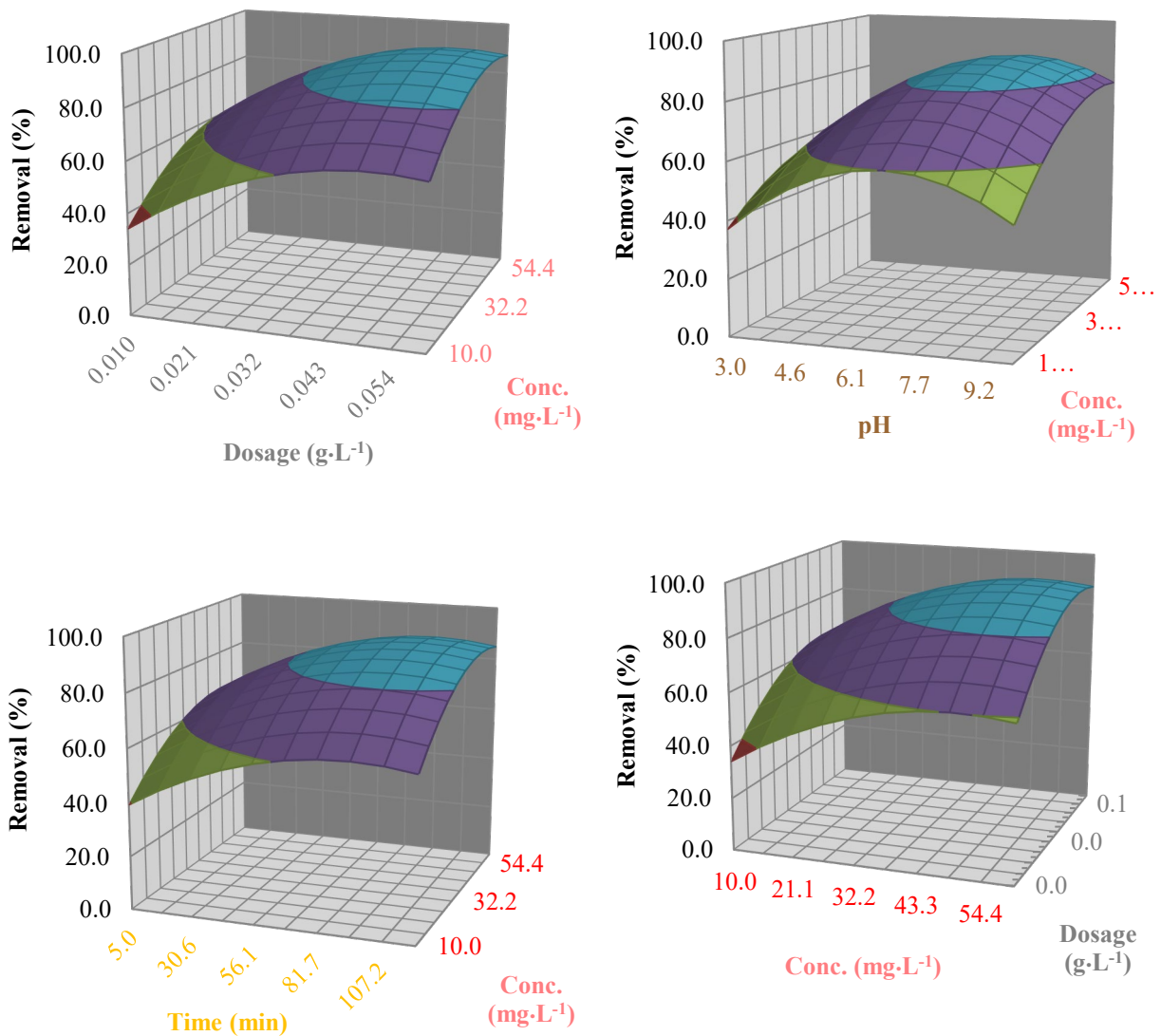


Figure 9. Response surface of full quadratic model between removal and variables to obtain an optimized system for adsorption of Cd(II) on synthesized ZIF-8; initial concentration of metal ion (F1), pH (F2), adsorbent dosage (F3) and contact time (F4).

3.3.2 Effect of adsorbent dosage

The adsorbent dosage is the key factor affecting the heavy metal ion adsorption efficiency. Hence, the adsorbent dosage in the range of $0.01 \text{ g}\cdot\text{L}^{-1}$ to $0.07 \text{ g}\cdot\text{L}^{-1}$ was investigated. The adsorption process and the adsorbent properties, such as surface area, cavities shape, and porosity, had a punctual effect on the adsorption efficiency. As shown in Figures 9-11, increasing the adsorbent dosage led to a higher adsorption efficiency of the heavy metal ions. When the adsorbent dosage reached more than $0.05 \text{ g}\cdot\text{L}^{-1}$, the adsorption did not significantly increase by ZIF-8 increment. This can be due to the agglomeration of the particles which leading to a decrease in the total surface area of the adsorbent [45,46]. According to the results, 0.05, 0.06, and $0.05 \text{ g}\cdot\text{L}^{-1}$ of synthesized ZIF-8 were chosen as the optimum amount of adsorbent for Cd(II), Ni(II), and Pb(II) metal ion adsorption from solution, respectively.

3.3.3 Effect of contact time

The role of contact time as an effective parameter on the adsorbed amount of Cd(II), Ni(II), and Pb(II) ions by the synthesized ZIF-8 in the range of 5 min to 120 min at room temperature was studied. The results are shown in Figure 9-11. It can be seen that the adsorption yield of heavy metal ions increased rapidly with the contact time because the vacant adsorption sites were abundant [47-49]. Based on the results, the contact times from 55 to 60, 45 to 60, and 50 to 90 were selected as the optimum contact time values for further experimental studies of Cd(II), Ni(II), and Pb(II) metal ion removal by synthesized ZIF-8, respectively. As can be expected, after a while, the lack of an active site led to a decreased adsorption rate, and finally, equilibrium was attained. Hence, the equilibrium time for metal ion adsorption was found to be 50 min, for all studied metal ions. After this time, no significant change in adsorption efficiency in the solution was observed.

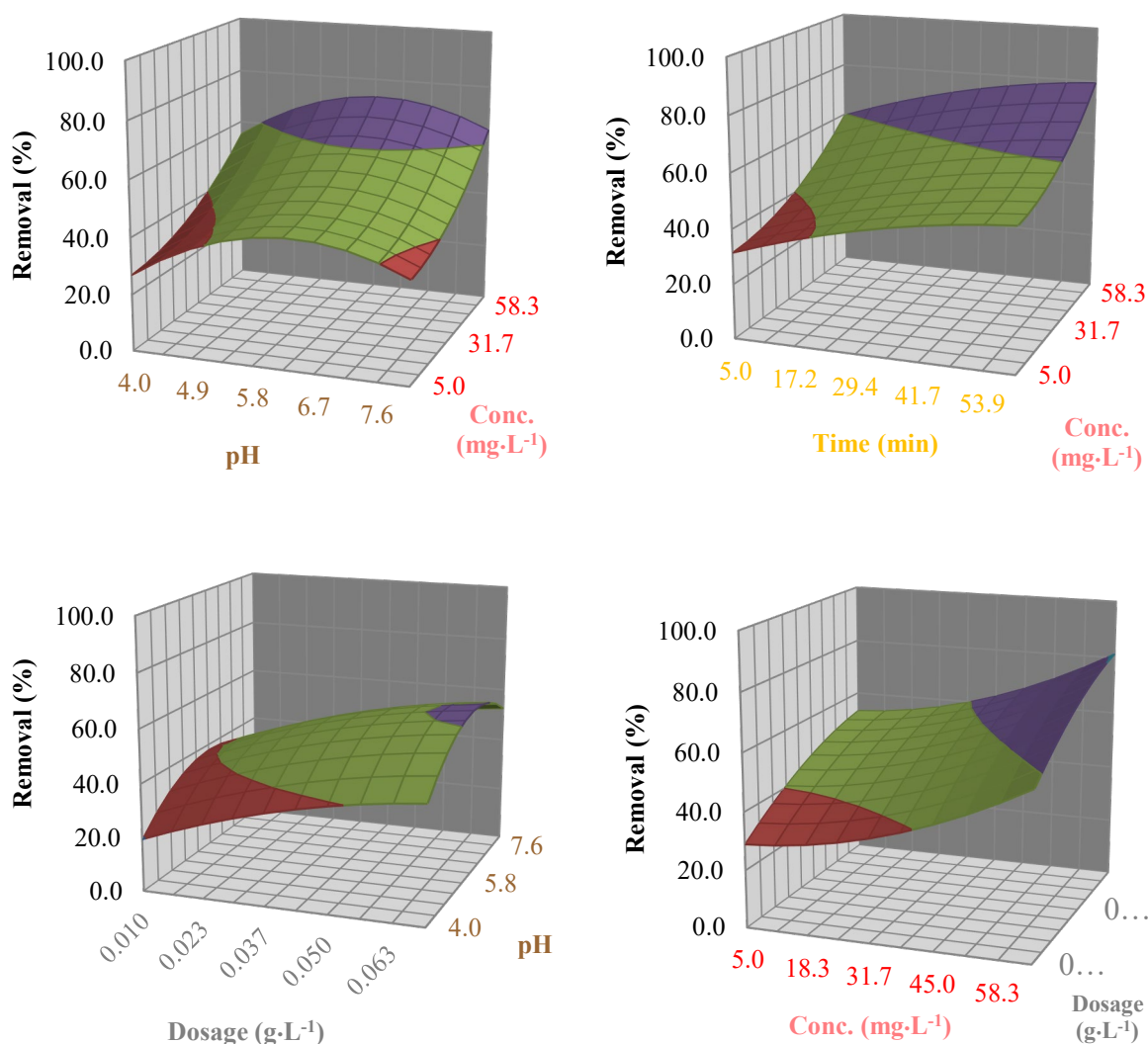


Figure 10. Response surface of full quadratic model between removal and variables in order to obtain optimized system for adsorption of Ni(II) on synthesized ZIF-8; initial concentration of metal ion (F1), pH (F2), adsorbent dosage (F3) and contact time (F4).

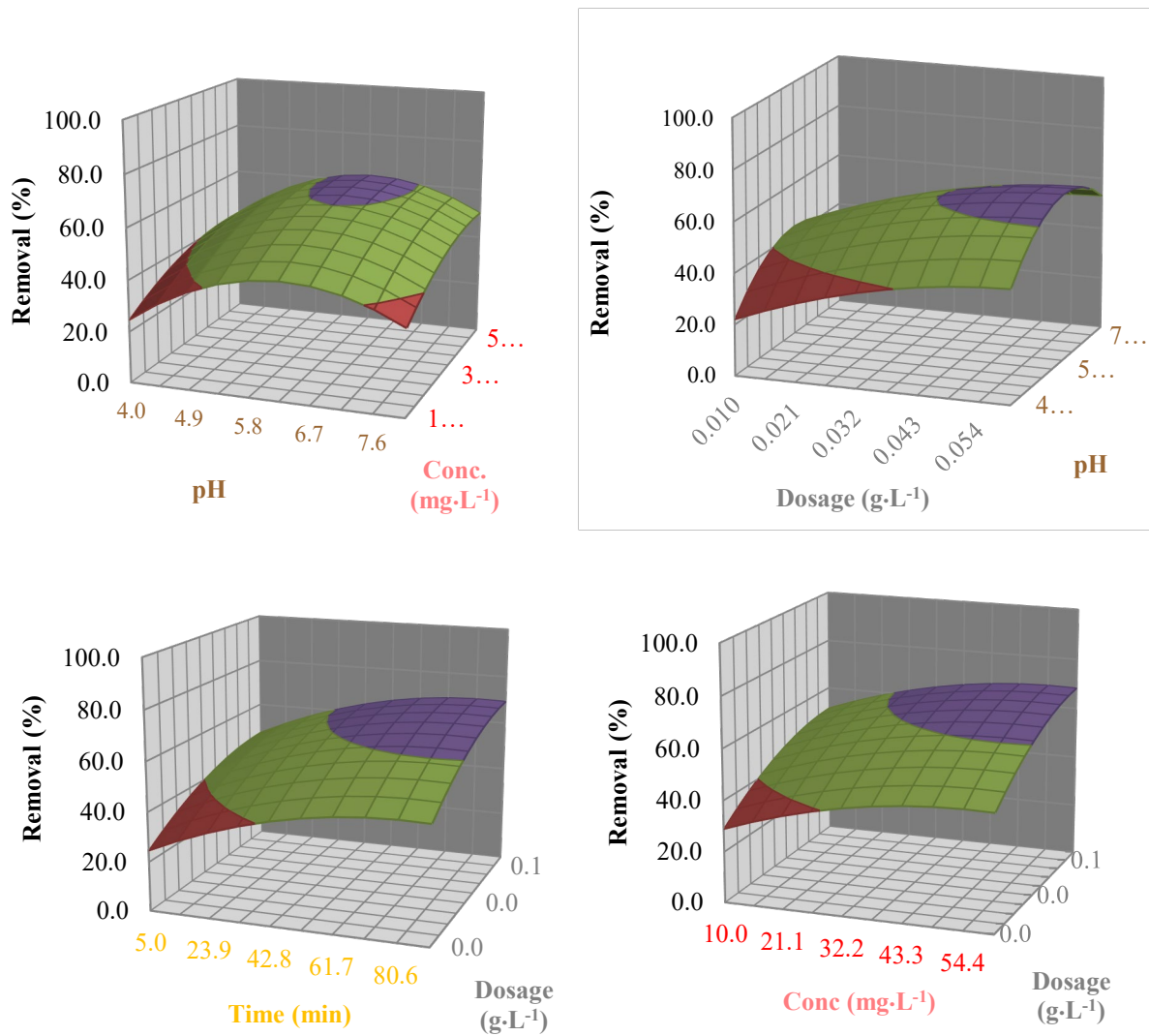


Figure 11. Response surface of full quadratic model between removal and variables in order to obtain optimized system for adsorption of Pb(II) on synthesized ZIF-8; initial concentration of metal ion (F1), pH (F2), adsorbent dosage (F3) and contact time (F4).

3.3.4 Effect of Initial concentration

Initial concentration is another notable factor in the adsorption process. In this study, the effect of the initial concentration of Cd(II), Ni(II), and Pb(II) metal ion (10 mg·L⁻¹ to 60 mg·L⁻¹) adsorption by the synthesized ZIF-8 was studied for 2 h at ambient temperature. As shown in Figures 9-11, the adsorption increased by increasing the metal ion concentration due to the increase in the driving force resulting from the increase of the pressure gradient concentration. Accordingly, at lower concentrations, the number of metal ions available in the solution was lower than the available sites on the adsorbent. Finally, adsorption was close to the saturation limit due to the finite active binding sites [50,51]. According to these results, the range of initial concentration from 45 mg·L⁻¹ to 55, 60 mg·L⁻¹ to 65, and 50 mg·L⁻¹ to 60 mg·L⁻¹ was selected as the optimum initial concentration values for further experimental studies of Cd(II), Ni(II) and Pb(II) metal ion removal by synthesized ZIF-8, respectively.

4. Conclusion

In this study, the adsorbent ZIF-8 synthesized by the solvothermal method was utilized for the removal of Cd(II), Ni(II), and Pb(II) ions from aqueous solutions. The best conditions for removing these metal ions were determined with RSM based on CCD, including the initial concentration of the metal ions, pH, adsorbent dosage, and contact time. For these cases, the R²adj was well within acceptable limits. There were no significant differences between the R² values, revealing that the experimental data exhibited a good fit with the third-order polynomial equations. The response surface plots showed the interaction between the mentioned factors when the remaining factors were fixed at a central point. The results showed a pronounced dependency of adsorption on all the investigated experimental variables. According to the achieved results, the aqueous solution pH values of 6.5, 6.5, and 6.0, adsorbent dosages of 0.05, 0.06, and 0.05 g·L⁻¹ to, and metal ions initial concentrations of 50, 60, and

60 mg·L⁻¹ were chosen as the optimum values of these variables for Cd(II), Ni(II) and Pb(II) metal ion adsorption from solution, respectively. After 50 min, 80% of the metal ions were adsorbed from the solution, and hence, the equilibrium time for metal ion adsorption was 50 min. The characterization results of the synthesized ZIF-8 adsorbent using XRD, FT-IR, BET, FE-SEM/EDX, and TEM methods were as follows. The stronger XRD peaks at $2\theta = 7.4, 10.6, 13.1, 15.1, 16.6,$ and 18.2 correspond to planes (110), (200), (211), (220), (310), and (222), respectively, indicating a high crystallinity of the prepared ZIF-8. The FTIR spectra of ZIF-8 after ion metal adsorbing differed from those of the pristine ZIF-8. As a result, adsorption was the main process involved in the removal of all three metal ions by the ZIF-8 nanocrystals. The Type I BET isotherm indicated the microporosity nature of the synthesized ZIF-8 with a surface area of 703.4 m²·g⁻¹ to, pore diameter of 1.2 nm, and total pore volume of 0.34 cm³·g⁻¹. The octahedral crystals of the synthesized ZIF-8 were visible from the FE-SEM analysis and had some cavities in their structure capable of uptaking metal ions. The elemental mapping analysis confirmed the EDS data and homogeneous dispersion of C, N, and Zn elements near and at the surface of the adsorbent. The analysis of the bulk synthesized ZIF-8 and its 3-dimensional shape displayed particles with nano size and sharp hexagonal faces. Based on the results, it can be suggested that the zeolite imidazolate framework (ZIF-8) has excellent potential as an effective adsorbent and used for heavy metal sorption from water environment

Acknowledgements

The authors appreciate the support provided by the Iranian Research Organization for Scientific and Technology (IROST) in conducting this research. The editing provided by Mr. Mohammad Fakhrizadeh is greatly appreciated.

References

- [1] D. Witkowska, J. Słowik, and K. Chilicka, "Heavy metals and human health: Possible exposure pathways and the competition for protein binding sites," *Molecules*, vol. 26, pp. 1-16, 2021.
- [2] H. A. Al-Swadi, A. R. Usman, A. S. Al-Farraj, M.I. Al-Wabel, M. Ahmad, and A. Al-Faraj, "Sources, toxicity potential, and human health risk assessment of heavy metals-laden soil and dust of urban and suburban areas as affected by industrial and mining activities," *Scientific Reports*, vol. 12, pp.1-18, 2022.
- [3] M. Balali-Mood, K. Naseri, Z. Tahergorabi, M.R. Khazdair, M. Sadeghi, "Toxic mechanisms of five heavy metals: mercury, lead, chromium, cadmium, and arsenic," *Frontiers in pharmacology*, vol. 12, p. 643972, 2021.
- [4] R.K. Sharma, and M. Agrawal, "Biological Effects of Heavy Metals: An Overview," *Journal of Environmental Biology*, vol. 26, pp. 301-313, 2005.
- [5] K. Li, N. Miwomunyuie, L. Chen, H. Jingyu, P. S. Amaniampong, D. Ato Koomson, D. Ewusi-Mensah, W. Xue, G. Li, and H. Lu, "Sustainable application of ZIF-8 for heavy-metal removal in aqueous solutions," *Sustainability*, vol. 13, no. 2, p. 984, 2021.
- [6] R. Abdeldayem, "A preliminary study of heavy metals pollution risk in water," *Applied Water Science*, vol. 10, pp. 1-4, 2020.
- [7] E. B. Silva, I. S. Alves, L. R. F. Alleoni, P. H. Graziotti, M. M. M. Farnezi, L. L. Santos, J. T. Prochnow, and I. C. I. Fontan, "Availability and toxic level of cadmium, lead and nickel in contaminated soils," *Communications in Soil Science and Plant Analysis*, vol. 51, no. 10, pp. 1341-1356, 2020.
- [8] N. A. Qasem, R. H. Mohammed, and D. U. Lawal, "Removal of heavy metal ions from wastewater: A comprehensive and critical review," *Npj Clean Water*, vol. 4, no. 1, pp. 1-15, 2021.
- [9] B. Chen, Z. Yang, Y. Zhu, and Y. Xia, "Zeolitic imidazolate framework materials: recent progress in synthesis and applications," *Journal of Materials Chemistry A*, vol. 2, no. 40, pp. 16811-16831, 2014.
- [10] Y. Zhang, Z. Xie, Z. Wang, X. Feng, Y. Wang, and A. Wu, "Unveiling the adsorption mechanism of zeolitic imidazolate framework-8 with high efficiency for removal of copper ions from aqueous solutions," *Dalton Transactions*, vol. 45, no. 32, pp.12653-12660, 2016.
- [11] M. Niknam Shahrak, M. Ghahramaninezhad, and M. Eydifarash, "Zeolitic imidazolate framework-8 for efficient adsorption and removal of Cr(VI) ions from aqueous solution," *Environmental Science and Pollution Research*, vol. 24, no. 10, pp. 9624-9634, 2017.
- [12] Y. Zhang, Z. Xie, Z. Wang, X. Feng, Y. Wang, and A. Wu, "Unveiling the adsorption mechanism of zeolitic imidazolate framework-8 with high efficiency for removal of copper ions from aqueous solutions," *Dalton Transactions*, vol. 45, no. 32, pp. 12653-12660, 2016.
- [13] A. Tanihara, K. Kikuchi, and H. Konno, "Insight into the mechanism of heavy metal removal from water by mono-disperse ZIF-8 fine particles," *Inorganic Chemistry Communications*, vol. 131, p. 108782, 2021.
- [14] Y. Chen, and S. Tang, "Solvothermal synthesis of porous hydrangea-like zeolitic imidazole framework-8 (ZIF-8) crystals," *Journal of Solid State Chemistry*, vol. 276, pp. 68-74, 2019.
- [15] A. A. Tezerjani, R. Halladj, and S. Askari, "Different view of solvent effect on the synthesis methods of zeolitic imidazolate framework-8 to tuning the crystal structure and properties," *RSC advances*, vol. 11, no. 32, pp. 19914-19923, 2021.
- [16] F. Hillman, J.M. Zimmerman, S.M. Paek, M.R. Hamid, W.T. Lim, H.K. Jeong, "Rapid microwave-assisted synthesis of hybrid zeolitic-imidazolate frameworks with mixed metals and mixed linkers," *Journal of Materials Chemistry A*, vol. 5, no. 13, pp. 6090-6099, 2017.
- [17] S. Nalesso, G. Varlet, M. J. Bussemaker, R. P. Sear, M. Hodnett, R. Monteagudo-Oliván, V. Sebastián, J. Coronas, and J. Lee, "Sonocrystallisation of ZIF-8 in water with high excess of ligand: Effects of frequency, power and sonication time," *Ultrasonics Sonochemistry*, vol. 76, p. 105616, 2021.
- [18] P. Ji, R. Tian, H. Zheng, J. G. Jiang, J. Sun, and J. Peng, "Solvent-free synthesis of ZIF-8 from zinc acetate with the assistance of sodium hydroxide," *Dalton Transactions*, vol. 49, no. 36, pp. 12555-12558, 2020.
- [19] P. Ji, X. Hu, R. Tian, H. Zheng, J. Sun, W. Zhang, and J. Peng, "Atom-economical synthesis of ZnO@ZIF-8 core-shell heterostructure by dry gel conversion (DGC) method for enhanced

- H₂ sensing selectivity,” *Journal of Materials Chemistry C*, vol. 8, no. 8, pp. 2927-2936, 2020.
- [20] O. Kolmykov, J.M. Commenge, H. Alem, E. Girot, K. Mozet, G. Medjahdi, and R. Schneider, “Microfluidic reactors for the size-controlled synthesis of ZIF-8 crystals in aqueous phase,” *Materials & Design*, vol. 122, pp. 31-41, 2017.
- [21] K. S. Park, Z. Ni, A. P. Côté, J. Y. Choi, R. Huang, F. J. Uribe-Romo, H. K. Chae, M. O’Keefe, and O. M. Yaghi, “Exceptional chemical and thermal stability of zeolitic imidazolate frameworks,” *Proceedings of the National Academy of Sciences*, vol. 103, no. 27, pp. 10186-10191, 2006.
- [22] T. Lundstedt, E. Seifert, L. Abramo, B. Thelin, A. Nystrom, J. Pettersen, and R. Bergman, “Experimental design and optimization,” *Chemometrics and Intelligent Laboratory Systems*, vol. 42, no. 1-2, pp. 3-40, 1998.
- [23] A. Khosravi, M. Esmhosseini, J. Jalili, and S. Khezri, “Optimization of ammonium removal from waste water by natural zeolite using central composite design approach,” *Journal of Inclusion Phenomena and Macrocyclic Chemistry*, vol. 74, pp. 383-390, 2012.
- [24] H. Y. Jang, J. K. Kang, J. A. Park, S. C. Lee, and S. B. Kim, “Metal-organic framework MIL-100(Fe) for dye removal in aqueous solutions: Prediction by artificial neural network and response surface methodology modeling,” *Environmental Pollution*, vol. 267, p. 115583, 2020.
- [25] M. Darvishmotevalli, A. Zarei, M. Moradnia, M. Noorisepehr, and H. Mohammadi, “Optimization of saline wastewater treatment using electrochemical oxidation process: prediction by rsm Method,” *MethodsX*, vol. 6, pp. 1101-1113, 2019.
- [26] J. Cravillon, S. Münzer, S. J. Lohmeier, A. Feldhoff, K. Huber, and M. Wiebcke, “Rapid room-temperature synthesis and characterization of nanocrystals of a prototypical zeolitic imidazolate framework,” *Chemistry of Materials*, vol. 21, no. 8, pp. 1410-1412, 2009.
- [27] Y. J. Zhang, Z. Q. Xie, Z. Q. Wang, X. H. Feng, Y. Wang, and A. G. Wu, “Unveiling the adsorption mechanism of zeolitic imidazolate framework-8 with high efficiency for removal of copper ions from aqueous solutions,” *Dalton Transactions*, vol. 45, no. 32, pp. 12653-12660, 2016.
- [28] Z. Lian, L. Huimin, and O. Zhaofei, “In situ crystal growth of zeolitic imidazolate frameworks (ZIF) on electrospun polyurethane nanofibers,” *Dalton Trans*, vol. 43, pp. 6684-6688, 2014.
- [29] U. P. N. Tran, K. K. A. Le, and N. T. S. Phan, “Expanding applications of metal organic frameworks: zeolite imidazolate framework zif-8 as an efficient heterogeneous catalyst for the knoevenagel reaction,” *ACS Catalysis*, vol. 1, pp. 120-127, 2011.
- [30] C. S. Wu, Z. H. Xiong, C. Li, and J. M. Zhang, “Zeolitic imidazolate metal organic framework ZIF-8 with ultra-high adsorption capacity bound tetracycline in aqueous solution,” *RSC Advances*, vol. 5, pp. 82127-82137, 2015.
- [31] H. L. Jiang, B. Liu, T. Akita, M. Haruta, H. Sakurai, and Q. J. Xu, “Au@ZIF-8: CO oxidation over gold nanoparticles deposited to metal-organic framework,” *Journal of the American Chemical Society*, vol. 131, pp. 11302-11303, 2009.
- [32] Z. Öztürk, M. Filez, and B. M. Weckhuysen, “Decoding nucleation and growth of zeolitic imidazolate framework thin films with atomic force microscopy and vibrational spectroscopy,” *Chemistry—A European Journal*, vol. 23, no. 45, pp. 10915-10924, 2017.
- [33] Y. Ding, Y. Xu, B. Ding, Z. Li, F. Xie, F. Zhang, H. Wang, J. Liu, and X. Wang, “Structure induced selective adsorption performance of ZIF-8 nanocrystals in water,” *Colloids and Surfaces A: Physicochemical and Engineering Aspects*, vol. 520, pp. 661-667, 2017,
- [34] E. Binaician, S. Maleki, N. Motaghedi, and M. Arjmandi, “Study on the performance of Cd²⁺ sorption using dimethyl-ethylenediamine-modified zinc-based MOF (ZIF-8-mmen): optimization of the process by RSM technique,” *Separation Science and Technology*, vol. 55, pp. 2716-2728, 2020.
- [35] Y. J. Zhang, Z. Q. Xie, Z. Q. Wang, X. H. Feng, Y. Wang, and A. G. Wu, “Unveiling the adsorption mechanism of zeolitic imidazolate framework-8 with high efficiency for removal of copper ions from aqueous solutions,” *Dalton Transactions*, vol. 45, no. 32, pp. 12653-12660, 2016.
- [36] S. J. Hoseini, M. Bahrami, and S. M. Nabavizadeh, “ZIF-8 nanoparticles thin film at an oil–water interface as an electrocatalyst for the methanol oxidation reaction without the application of noble metals,” *New Journal of Chemistry*, vol. 43, pp. 15811-15822, 2019.
- [37] Y. Pan, Y. Liu, G. Zeng, L. Zhao, and Z. Lai, “Rapid synthesis of zeolitic imidazolate framework-8 (ZIF-8) nanocrystals in an aqueous system,” *Communications chemistry*, vol. 47, pp. 2071-2073, 2011.
- [38] A. F. Gross, E. Sherman, and J. J. Vajo, “Aqueous room temperature synthesis of cobalt and zinc sodalite zeolitic imidazolate frameworks,” *Dalton Transactions*, vol. 41, pp. 5458-5460, 2012.
- [39] H. Esfandian, A. Akrami, and F. B. Shahri, “Application of response surface methodology (RSM) for optimization of strontium sorption by synthetic ppy/perlite nanocomposite,” *Desalination and Water Treatment*, vol. 93, pp. 74-82, 2017.
- [40] F. N. Chianeh, and J. B. Parsa, “Electrochemical degradation of metronidazole from aqueous solutions using stainless steel anode coated with SnO₂ nanoparticles: experimental design,” *Journal of the Taiwan Institute of Chemical Engineers*, vol. 59, pp. 424-432, 2016.
- [41] S. Wang, L. Bromberg, H. Schreuder-Gibson, and T. A. Hatton, “Organophosphorous ester degradation by chromium (III) terephthalate metal–organic framework (MIL-101) chelated to N, N-Dimethylaminopyridine and related aminopyridines,” *ACS Applied Materials & Interfaces*, vol. 5, pp. 1269-1278, 2013.
- [42] A. J. Howarth, Y. Liu, P. Li, Z. Li, T. C. Wang, J. Hupp, and O. Farha, “Thermal and mechanical stabilities of metal-organic frameworks,” *Nature Reviews Materials*, vol. 3, pp. 1-15, 2016.
- [43] M. P. Jian, B. Liu, G. S. Zhang, R. P. Liu, and X. W. Zhang, “Adsorptive removal of arsenic from aqueous solution by zeolitic imidazolate framework-8 (ZIF-8) nanoparticles,” *Colloids and Surfaces A: Physicochemical and Engineering Aspects*, vol. 465, pp. 67-76, 2014.

- [44] M. Roushani, Z. Saedi, and Y. Baghelani, "Removal of cadmium ions from aqueous solutions using TMU-16-NH₂ metal organic framework," *Environmental Nanotechnology, Monitoring and Management*, vol. 7, pp. 89-96, 2017.
- [45] A. Heidari, H. Younesi, and Z. Mehraban, "Removal of Ni(II), Cd(II), and Pb(II) from a ternary aqueous solution by amino functionalized mesoporous and nanomesoporous silica", *Chemical Engineering Journal*, vol. 153, pp. 70-79, 2009.
- [46] Y. X. Li, H. N. Zhang, Y. T. Chen, L. Huang, Z. A. Lin, and Z. W. Cai, "Core-shell structured magnetic covalent organic framework nanocomposites for triclosan and triclocarban adsorption," *ACS Applied Materials & Interfaces*, vol. 11, pp. 22492-22500, 2019.
- [47] C. G. Lee, J. W. Jeon, M. J. Hwang, K. H. Ahn, C. Park, J. W. Choi, and S. H. Lee, "Lead and copper removal from aqueous solutions using carbon foam derived from phenol resin," *Chemosphere*, vol. 130, pp. 59-65, 2015.
- [48] E. Cerrahoğlu, A. Kayan, and D. Bingöl, "Multivariate optimization for removal of some heavy metals using novel inorganic-organic hybrid and calcined materials," *Separation Science and Technology*, vol. 53, pp. 2563-2572, 2018.
- [49] M. R. Awual, "A novel facial composite adsorbent for enhanced copper(II) detection and removal from wastewater," *Chemical Engineering Journal*, vol. 266, pp. 368-375, 2015.
- [50] S. Kushwaha, H. Soni, V. Ageetha, and P. Padmaja, "An insight into the production, characterization, and mechanisms of action of low-cost adsorbents for removal of organics from aqueous solution," *Critical Reviews in Environmental Science and Technology*, vol. 43, pp. 443-549, 2013.
- [51] L. Ma, X. Zhang, M. Ikram, M. Ullah, H. Wu, and K. Shi, "Controllable synthesis of an intercalated ZIF-67/EG structure for the detection of ultratrace Cd²⁺, Cu²⁺, Hg²⁺ and Pb²⁺ ions," *Chemical Engineering Journal*, vol. 395, p. 125216, 2020.